LAWRENCE
LIVERMORE
NATIONAL
LABORATORY

UCRL-TR-212339

Gamma-Ray Imaging Measurements in the ORNL Radiochemical Engineering Development Center

K. P. Ziock

May 17, 2005

This work was performed under the auspices of the U.S. Department of Energy by University of California, Lawrence Livermore National Laboratory under Contract W-7405-Eng-48.

Gamma-Ray Imaging Measurements

in the ORNL

Radiochemical Engineering Development Center

Klaus-Peter Ziock
Lawrence Livermore National Laboratory

Abstract

This report describes gamma-ray imaging measurements conducted in the ORNL Radiochemical Engineering Development Center in response to the radiological event that occurred on March 2, 2005. A week-long campaign in the facility's limited access area did not reveal any new contamination sites. Successful images were obtained of a number of known sites of contamination. These can be used to provide upper bounds on new contamination in the images obtained. In addition, the perturbing effect of TRU waste drums on early images indicates that no major sites of contamination are present in the areas imaged. Finally, it is suggested that continual monitoring of the facility using gamma-ray images would be useful to establish a baseline for future events. This could be performed with a single imager that is cycle through a number of locations.

This work was performed under the auspices of the U.S. Department of Energy by University of California, Lawrence Livermore National Laboratory under Contract W-7405-Eng-48.

Overview

In response to a radiological event that occurred on March 2, 2005 at the ORNL Radiochemical Engineering Development Center (REDC) a request was made to bring the LLNL Gamma-Ray Imaging Spectrometer (GRIS) to the facility to search for radiological contamination due to the event. Dr. Klaus Ziock of LLNL agreed to bring the camera and participate in a week-long measurement campaign to try and find new sites of radiological contamination. This document reports on the results of that campaign, providing information on the imaging system, how it was deployed and the results from measurements made in the facility. In addition, recommendations on how to improve long term monitoring of current hot spots and new ones from future events is discussed.

Instrumentation

The LLNL GRIS, shown in Fig. 1, has been described in detail in Ziock and Nakae. [1] The instrument comprises a coded-aperture imager that uses a rank-19, hexagonal, uniformly-redundant array that encodes the gamma-ray scene onto a position-sensitive, CsI(Na) scintillator-based detector. The instrument provides energy resolution commensurate with that obtained in a NaI(Tl) detector over an energy range from 20 keV to 630 keV. The data is recorded in list mode during the accumulation and is thus available for detailed analysis at the conclusion of the measurement. A demountable visible-light camera aligned on the gamma-ray imaging axis is used to obtain a visible-light image before an acquisition is begun. Based on a measured distance to the likely gamma-ray source, the visible-light image is scaled to the size of the gamma-ray image. In the instrument's display, the two images are overlaid with the visible-light image presented in black and white "behind" the false-color gamma-ray image. Pixels in the gamma-ray image below a selectable threshold level are turned clear so that the location of radiation "hot-spots" can be located with reference to the visible-light image (see Fig. 2.)

The resolution, dx of the gamma-ray image is determined from the simple formula:

$$dx = \frac{a}{f} d \qquad (1).$$

Where a is the base hole size in the aperture, f is the spacing between the detector and the mask and d is the distance to the source. The imager has five different selectable focal lengths, providing a zoom capability. This allows one some freedom in positioning the camera while retaining the ability to obtain reasonable spatial resolution at a hot-spot.

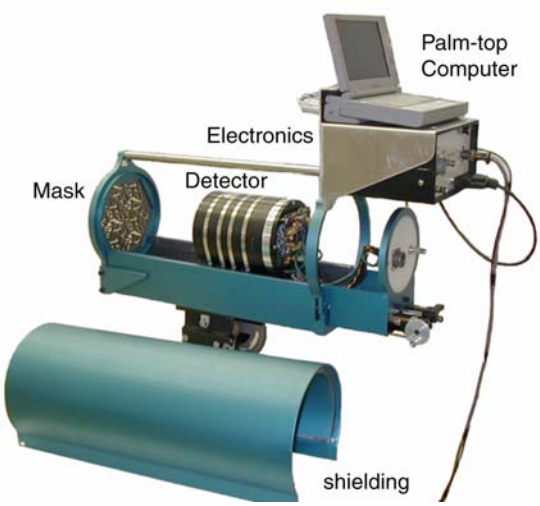

Fig.1. Current generation imager. The unit is battery powered and provides variable zoom images.

The energy resolution provided by the imager allows one to generate images from different parts of the spectrum. Up to four regions of interest can be set before an acquisition. An individual image is generated based on the data in each of the regions of interest as the data is collected. Post processing of the data creates a full data cube allowing the user to select different regions of interest without replaying the data. In addition, the spectra from different pixels or regions of the image can also be generated, [2] potentially allowing one to identify local isotopic content. (Fig. 2)

Applicaton details of Coded aperture imaging

The gamma-ray data is collected in two equal-time integrations. Between integrations the coded-aperture is rotated through 60 degrees about its center, effectively inverting the mask pattern. The two data sets are combined so as to remove background variations in counts-versus-position across the detector that are not due to the mask. Such variations are invariably present and are due to both residual non-linearities in the detector and due to scatter of the gamma-rays off of material near the detector. Although the variations are known to be scene specific, this procedure robustly removes them.

One can view coded aperture imaging as a pinhole camera with more than one pinhole to let in radiation from the source. Unlike a true imager that focuses radiation onto the detector, the image generation process for a coded-aperture imager uses all of the data in the detector to obtain the value at each point of the image. This has sensitivity implications as follows:

1) Performance is an order of magnitude better than a pinhole camera when small regions of

the field of view are significantly more radioactive than the rest of the field of view.

2) In the limit where the whole field glows equally, the sensitivity reverts approximately to that of a normal pinhole camera. [3]
3) In a scene with both strong and weak sources, the strong sources dominate the statistical noise, requiring more integration time to see the weak sources.
4) Radiation sources just outside the primary field of view will show up on the opposite side of the image. Sources far from the primary field can also introduce significant artifacts into the image. These effects can be removed with design modifications not implemented in this imager since these affects are not of concern in the normal application space for this instrument.

Measurements

The imager arrived on 4/12/05 without damage at ORNL and was successfully unpacked and turned on. It was known on shipment that slight alignment errors existed between the gamma-ray and video images. These were corrected by imaging a ^{166m}Ho source (see Fig. 3) After some discussions of likely locations to find hot spots, the imager was taken to the upper level of the Limited Access Area (LAA) of the facility.

Upper Level wall to chemical make up area

The first location imaged was the wall adjacent to the make-up area where an old spill on the far side of the wall had contaminated the wall. A quick integration of 10 minutes, 3 meters from the wall revealed no obvious contamination. (See Fig. 4) A longer integration was set over the lunch hour. Unfortunately, the imager was set to run off of its battery and this was too discharged to provide full performance over the second half of the integration. The resulting data showed that the energy response had sagged (peak at 0 keV) and the image showed systematic structure commensurate with an unbalanced mask/anti-mask acquisition. Even a partial replay of ~ ¼ of each of the runs showed the same affect so that the data is considered unsalvageable and is not shown.

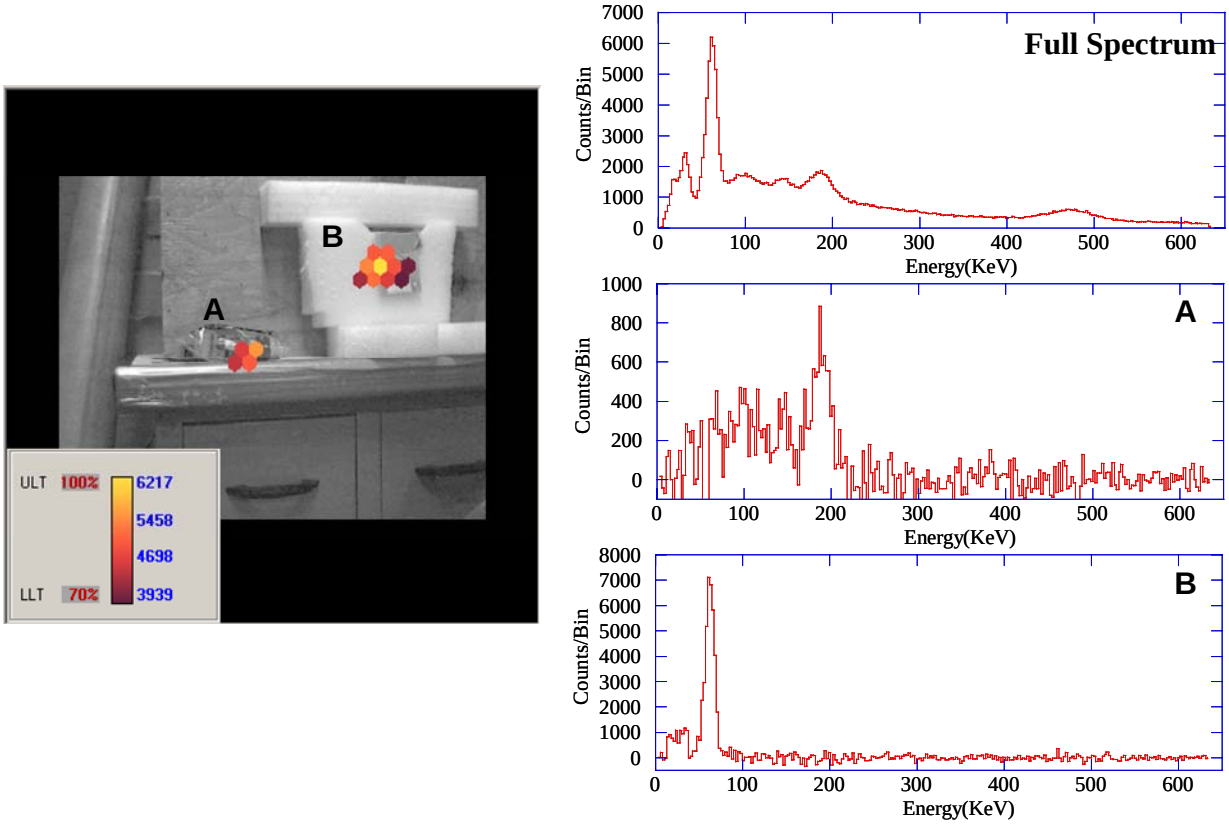

Fig. 2. The standard gamma-ray imager data as it is presented in the report. This image shows two point sources, HEU (A) and ^{241}Am (B.) The gamma-ray image is scaled to the video image and pixels below 70% peak intensity are turned clear so that the visible-light image can be seen for reference. This data was taken with the widest gamma-ray field of view. In such data, the field of view of the visible-light image is less than that of the gamma-ray image; hence the black border about the former. The top spectrum is from all of the events collected by the imager. The lower spectra are for the "on" (colored) gamma-ray pixels associated with each source as labeled.

Old Waste Pipe on TDF Platform
The imager was then moved to areas of concern for the release. These are on the lower level of the LAA. We started with a 10-minute exposure of the end of the old waste pipe on the TDF platform. There was a significant background coming into the back of the imager from the access hatch to the pipe tunnel directly behind the imager. The instrument's battery was positioned to act as a shield before the exposure. The range was 2.9 m. No obvious source is visible in the image (Fig. 5.)

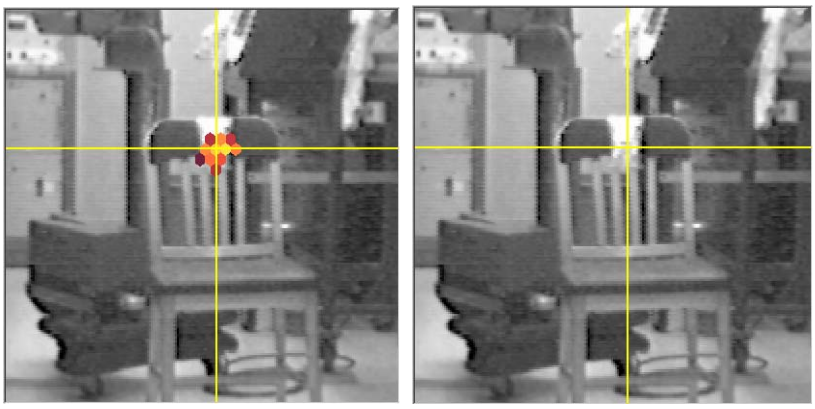

Fig. 3. Post alignment data. The composite gamma-ray/video image is shown on the left, the video only image is on the right. The cursor is located at the peak of the gamma-ray image.

A problem with video images occurred in this and the following three acquisitions. Due to the earlier battery problems, the computer lost the default video file size to save. Although images were recorded and they covered the same field of view as normal, the images saved were only one quarter of the normal pixel count. This lead to video-gamma scaling errors on the day the data was collected. The saved images have been expanded manually for correct scaling in this report. The primary effect of this is poorer resolution (and a slight possibility of a shift) in the video images. The problem was fixed for images taken the following day.

Access Hatch to pipe tunnel
For the next image, the instrument was swung around to look at the access hatch to the pipe tunnels. This image is shown in Fig. 6. It has two obvious features, intense point sources at opposite edges of the image. It was immediately recognized that this could be due to a single source at the edge of the field of view wrapping due to partial encoding (see imaging details # 4).

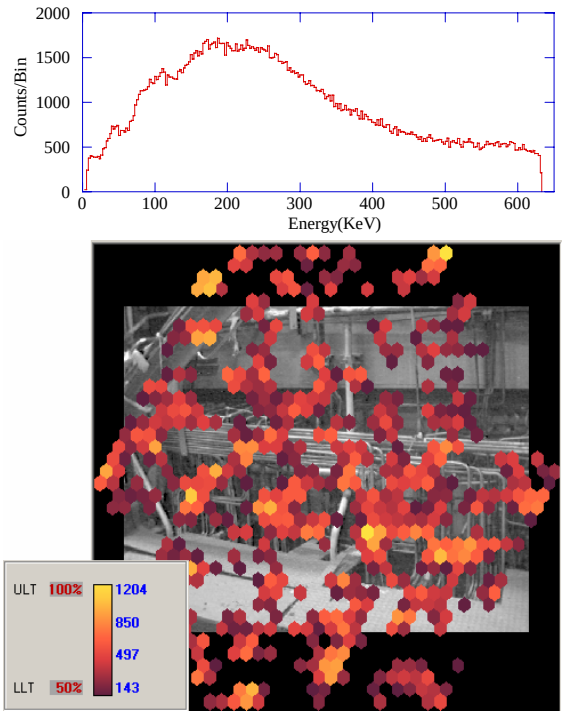

Fig. 4. Upper LAA wall image and spectrum. No obvious source is visible. Images formed with energy cuts of 60-129 keV, 130-211 keV and 212-631 keV also do not show significant structure.

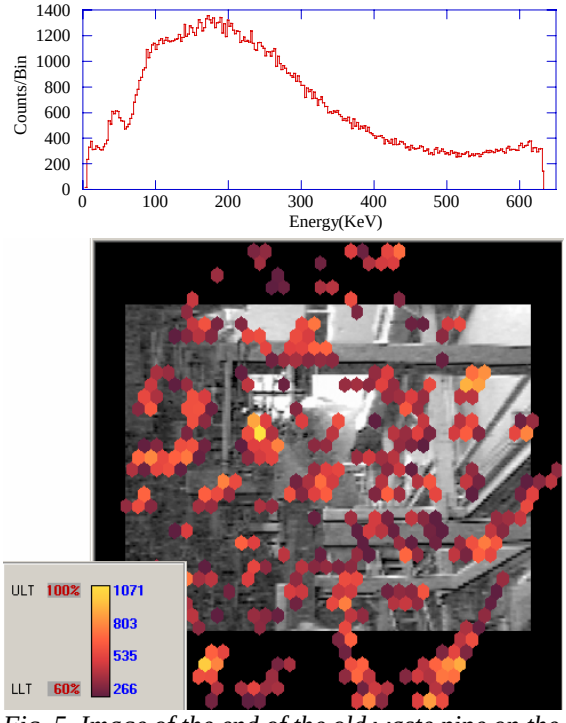

Fig. 5. Image of the end of the old waste pipe on the TDF platform. The threshold is set to 60% to allow the better orientation to the visible-light image. No obvious source is visible.

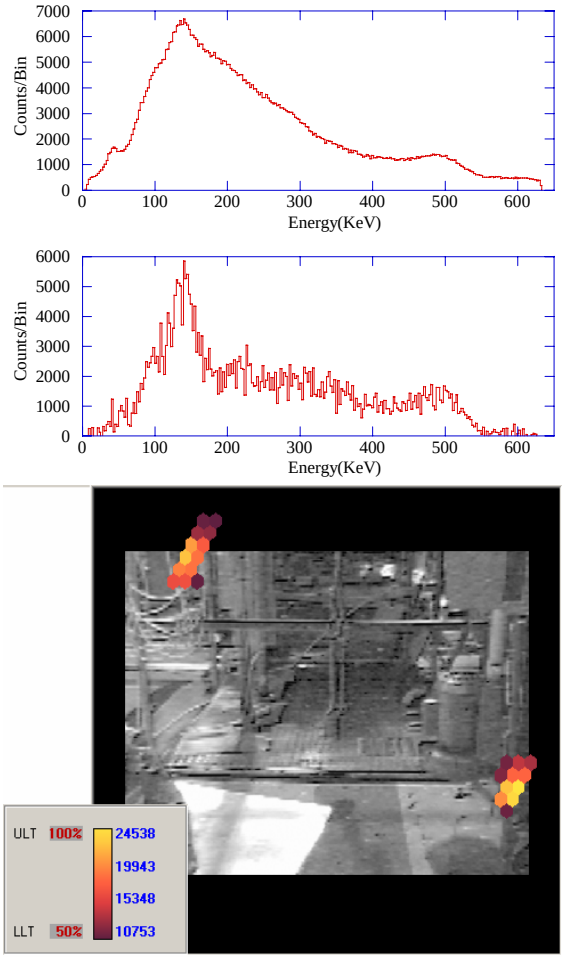

Fig. 6. Image of pipe gallery access hatch. The two spots are at the extreme edges of the gamma-ray field of view and are likely a single hot spot that is wrapped around the field by partial coding. The upper spectrum shows the full energy spectrum from the detector, the lower spectrum is only from the pixels above the gamma-ray threshold.

Hot Cell 7 wall

A scan of the cell walls to the right of the hatch with a hand probe indicated a hot spot on the right side of the previous image. The camera was re-aimed and a short exposure of the wall (4 min.) was taken. Although a possible extended source is shown, the significance is not high (Fig. 7.)

The imager aim was centered on the hot spot seen with the probe and the zoom increased to obtain a new image with higher statistics (30 mins.) The image is shown in Fig. 8. It is again suggestive of an extended source. However, subsequent analysis using different energy cuts did not change the significance of the image and the hot regions do not agree with those obtained in the previous wide-field image. This indicates that we are

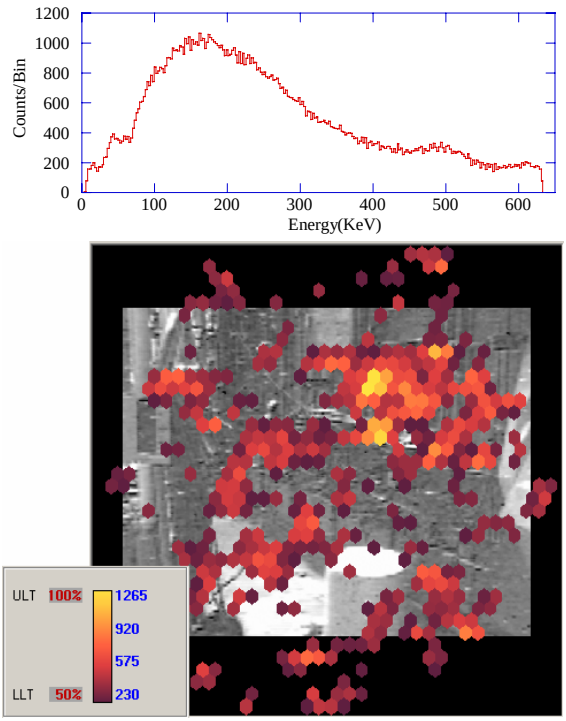

Fig. 7. Image of cell 7 wall hot-spot Although the image is suggestive of a distributed source, using various energy bands did not improve the contrast of the image.

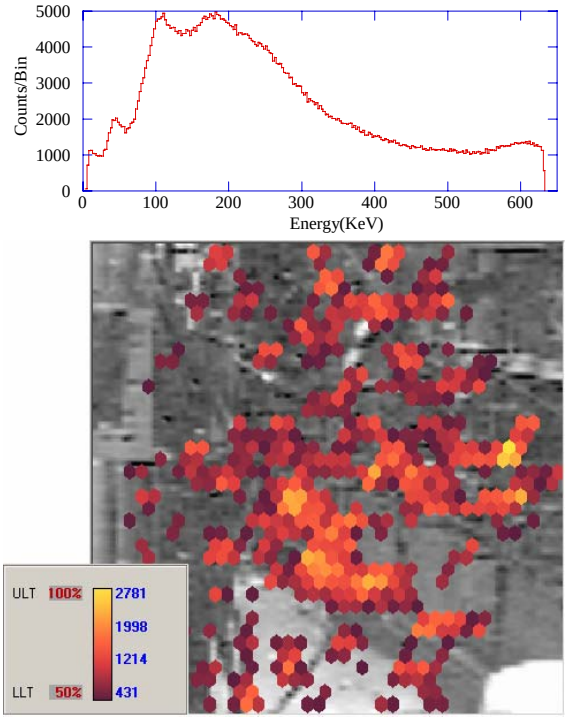

Fig. 8. Zoomed image of cell 7 wall hot-spot Although the image is suggestive of a distributed source, using various energy bands did not improve the contrast of the image.

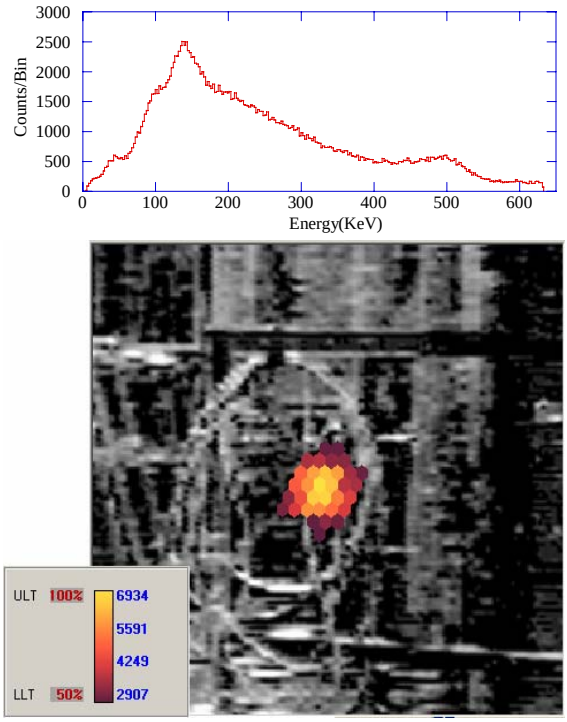

Fig. 9. Image taken to the left of the pipe tunnel access hatch. This is clearly the source seen split in two in the access hatch image, Fig. 6.

seeing artifacts, possibly due to a very strong source outside the primary field of view.

TRU waste drum

Since we did not find an obvious source to the right of the pipe-tunnel access hatch, we turned our attention to the left of the hatch. This time a significant source was seen in a short, 4-minute integration. It is shown in Fig. 9. The similarity of the spectrum, the sources location and its intensity indicates it is the hot spot that was just outside the field of view of the access hatch image (Fig. 6.) A scan with the hand instruments showed that there was a drum of waste material in this location, 8.3 m from the imager. It was so hot that it presumably dominated all of the images at this end of the LAA. In fact there were three drums of such waste, all found to be very hot when scanned with the hand probe. They made it extremely difficult to obtain images in this part of the LAA.

The following day the waste drums were removed and the rate looking toward the hatch was only 1100 counts/second compared with the previous day's rate of 1900 per second.

Hot Cell 4 Wall

For the first saved integration of the day, we went to a region of the cell wall by tank 4. This region was found to be hot with a hand scan and the radiation seemed to come from some wrapped pipes on the wall. At a distance of 2.9 m, a 40 minute integration was obtained. It is shown in Fig. 10. The image clearly reveals a hot region that appears to be offset from the pipe.

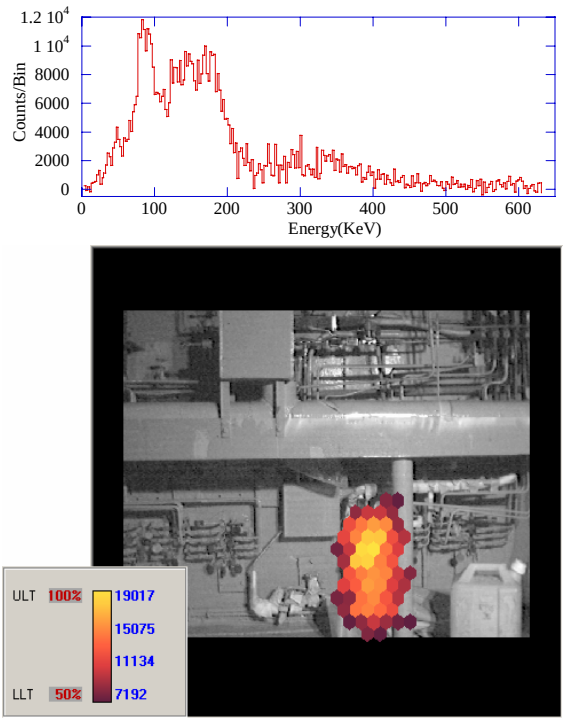

Fig. 10. Image of cell 4 wall hot-spot The image appears to show the contamination slightly to the right of the vertical pipe originally thought to be the source of the radiation. The energy spectrum is only from the gamma-ray pixels turned "on" in the image.

A zoomed image was taken later in the day to try to better localize the spot, i.e. to determine if it was really next to the pipe. A 30-minute integration at a range of

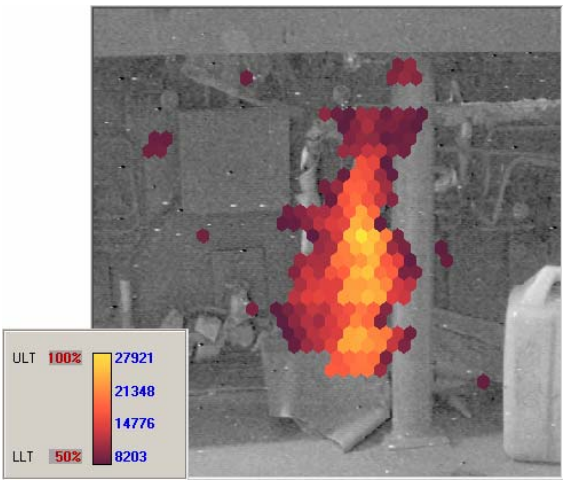

Fig. 11. Zoomed image of cell 4 wall hot-spot. The contamination is clearly not associated with the pipe. The spectrum is similar to that of Fig. 10 and is not shown.

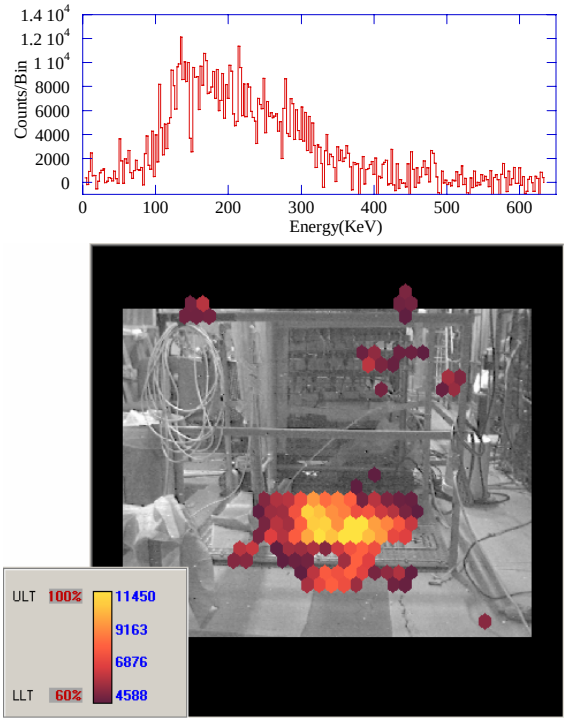

Fig. 12. Revisit of pipe tunnel access hatch. The threshold is set to 60%. The spectrum is from the on-only pixels.

2.5 m and at zoom of 2 was used (Fig. 11.) This means that the pixels in the image are 5.8 cm high (tip-to-tip) by 5.4 cm wide (flat-to-flat.) This image clearly shows that the contamination is not associated with the pipes.

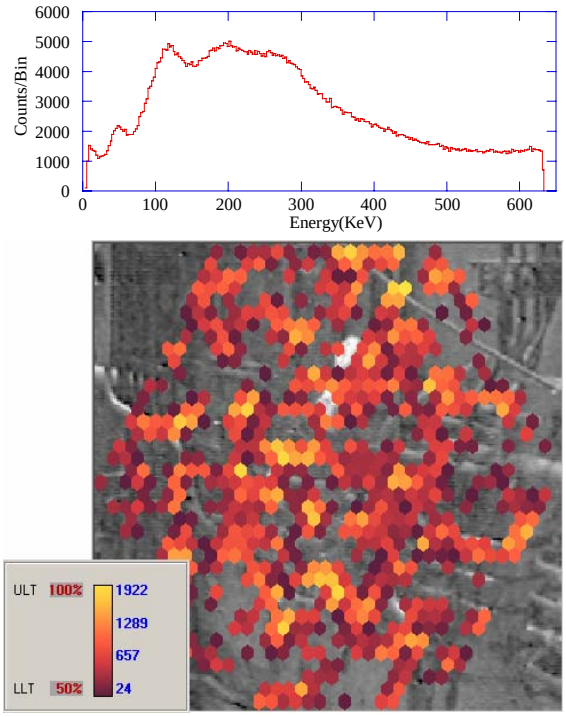

Fig. 13. Image of lower, cell-7 wall revisited. A well balanced run with no obvious source is seen.

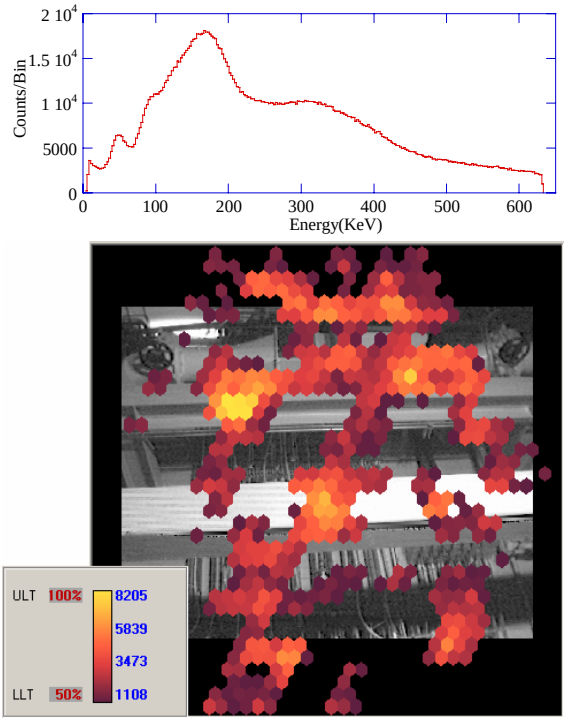

Fig. 14. Image of cell 4 HEPA Filter. The structure is due to partially encoded radiation from the hot region imaged in Fig's 9 and 10 and is not thought to represent a source in the field of view.

Pipe Tunnel Hatch (Revisited)

With the TRU barrels removed, we returned to the pipe tunnel access hatch and the cell-wall behind cell 7. A 30-minute exposure of the hatch cover taken from 2.9 meters produced the image in Fig. 12. The hatch is clearly imaged as a hot spot.

Lower Cell 7, Cell Wall

Additional images of the hot spot on the back wall of cell 7 were collected. Two separate images comprising a total of 40 minutes integration time were run. The combined results are shown in Fig. 12. Again, no obvious source is visible in the image. Various cuts on the energy spectrum do not provide any additional refinement to the image.

Cell Wall HEPA Filters

We next turned the imager on the HEPA filters mounted high on the cell walls. We started with the filter for cell 4 since this was the current imager location. A 90-minute exposure was taken from a range of 4 m. The results are shown in Fig. 14. The image has structure commensurate with a bad image. A careful evaluation of the geometry indicates that the hot region imaged in the previous exposure (Fig. 10) serves as a partially encoded source that is the likely source of the structure.

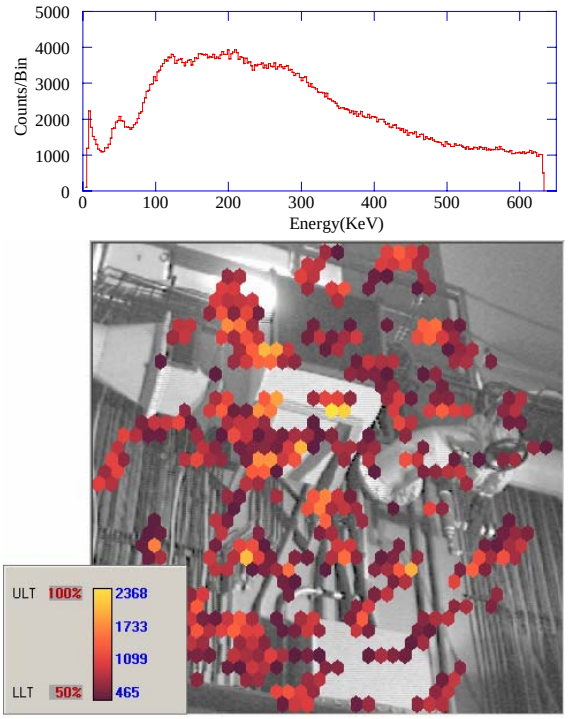

Fig. 15. Image of cell 6 HEPA filter box. No source is present.*

To get a "clean" picture of one of the HEPA filter boxes we moved the imager to look at the filter above

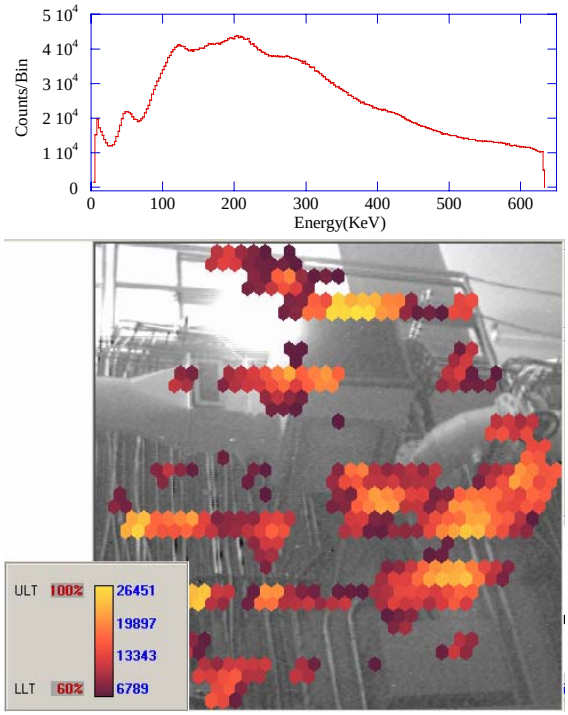

Fig. 16. Image of cell run 4/14/05-8 Overnight HEPA filter. Clearly noise dominated. Cuts on the different regions of the spectrum provide no improvement to the image.

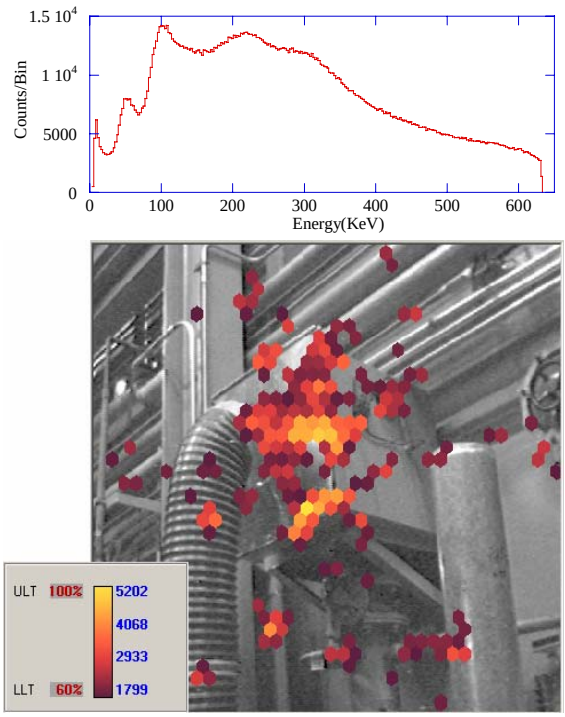

Fig. 16. Image of pipe tunnel HEPA filter. Some structure in 160-260 keV band. With slight structure in the 260-650 band.

hot cell 6. The imager axis was approximately perpendicular to all known sources (primarily the pipe tunnel hatch) in the area. At this location we took a one hour exposure at a distance of 4.5 m from the filter box. The image is shown in Fig. 15 and shows no obvious source. Energy cuts on the different regions of the spectrum also showed no obvious source.

Since the filter showed activity with a hand probe (although only of low energy or beta radiation, as the radiation could not penetrate the back-side of the pancake-probe) an overnight exposure (12 hours total) was setup. The results are shown in Fig. 16. These are disappointing in that they again show systematic structure. This persists despite applying various energy cuts on the structure in the spectrum. The source of the systematic noise is unknown. Personnel shifting materials in the field of view of the camera or near the camera could have changed the radiation environment. Alternately, we note that it has been a long time since the imager was calibrated. It appears that detector non-linearities have increased since the calibration occurred. This makes the imager more sensitive to imbalanced mask/anti-mask acquisitions since the systematic perturbations in each of the separate images is larger. Thus, even small changes in electronic gains due to thermal drifts could imbalance the image.

Pipe Tunnel HEPA Filter
The final exposure of the campaign was taken of the pipe-tunnel HEPA filter. A 2-hour exposre from a distance of 3.21 m provided the image shown in Fig. 17. Activity is clearly associated with the filter. The spectrum from the entire data set is shown, rather than that from only the pixels above-threshold (set at 60%.) The "on-pixels" spectrum has poor counting statistics and shows none of the structure of the full spectrum. It rises and falls slowly from a maximum at ~ 250 keV This is commensurate with the results that energy cuts on the various parts of the spectrum do not significantly enhance the image.

Conclusions
The primary conclusion to be drawn from the measurement campaign is that no significant new sources of contamination were found with the gamma-ray imager. Although the imager sensitivity is not absolutely calibrated, the various images obtained can be used to determine the approximate sensitivity of the approach. The first observation that can be drawn is that none of the observed radiation hot spots came anywhere near the leakage flux from the TRU drums. When present, this material totally dominated all measurements near the high-cell-number end of the LAA.

An estimate of the significance of the detection in a single pixel can be made by taking the standard deviation of the background level (deviation from the mean value of all pixels excluding high pixels) and dividing this into the peak pixel.

Using this procedure, the single TRU waste barrel in the field of view showed up in the short 4-minute exposure and at a range of 8.3 m with ~ 12 sigma significance. The next brightest source observed was the lower part of the cell-4 wall. This showed a significance of ~ 8 sigma for a 20 minute exposure while the pipe tunnel access hatch was only ~ 6.4 sigma for a 30 minute exposure. The significance estimate makes less sense as the source becomes more distributed and is less well differentiated from the background since selecting the "background" pixels becomes more difficult. As such, it does not make sense to apply it to any of the weaker detections.

It is interesting to see that the spectra from the weak or no source detection are similar in nature. The peak at ~ 75 keV is presumably the K-shell fluorescence radiation from the lead and tungsten shielding around the detector. The remaining spectral structure is real, although it is not associated with any obvious source and seems to be pervasive in the LAA environment. Spectral information is obtained from the "on" pixels of the strong detections. The only feature that stands out is the ~ 90 keV peak from the contamination on the cell-4 wall.
There are obvious regions of contamination that were not seen by the imager. Notably the contamination on the lower part of the cell-7 wall and the cell-wall-mounted HEPA filters. All of these were seen with the pancake probe of the hand-held detector, but only with the "window" facing the contamination. This indicates that these are very low energy x-ray sources or beta radiation. As the imager performance degrades at low energies, it is possible that low energy x-rays are present. The imager has not been tested much below 60 keV. A 125 μm Al window cuts off the detector response below ~ 10 keV and the degrading position resolution with energy will not provide much contrast below ~ 30 keV. The detector entrance window is presumably thick enough to keep it from seeing beta radiation.

The value of the gamma-ray images would be significantly enhanced if a baseline set of images existed. As releases are obviously infrequent events, one might plan a strategy to incorporate regular imaging data into the facility operations. A small imager, left for a day-long exposure, could obtain sensitive images. By cycling through a number of locations, one could cover the entire LAA over a period of order 10 days. By comparing sequential exposures of the same LAA regions one could look for changes in the contamination with time. This would provide a valuable resource following a release. It might also serve as a warning to help avert a major release if small problems are caught early on. Whether this function could be filled by extant commercial imagers or if a custom unit would better serve the facilities needs would require further study of both the radiation environment in the LAA and the normal facility operations.

References

1. *A Large-Area PSPMT Based Gamma-ray Imager with Edge Reclamation,* K.P. Ziock, L. Nakae,. IEEE Trans. Nuclear Science, **49**, 1552-1559, 2002.
2. *Real time generation of images with pixel-by-pixel spectra for a coded aperture imager with high spectral resolution,* K.P. Ziock, M.T. Burks, W. Craig, L. Fabris, E.L. Hull, N.W. Madden, , NIM B, ***505**, 420-424, 2003.*
3. *Coded aperture imaging: predicted performance of uniformly redundant arrays*, E.E. Fenimore, App. Opt., **17**, 3562-3570, 1978.